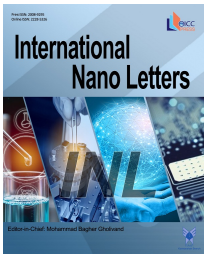

Volume 14, Issue 2, 142408 (1-13)

International Nano Letters (INL)

https://doi.org/10.57647/inl.2024.1402.08

Synergistic Effect of Nano-TiO_2 and CNTs on the Mechanical and Microstructural Properties of Cement–Silica Fume Stabilized Soils under Freeze–Thaw Cycles

Hamed Ajorloo[1], S. Mohammad Mirhosseini[1,*], Emadaldin Hezavehi[2], Ali Hassani Joshaghani[3]

[1]*Department of Civil Engineering, Ar.C., Islamic Azad University, Arak, Iran.*
[2]*Department of Textile Engineering, Ar.C., Islamic Azad University, Arak, Iran.*
[3]*Department of Chemical Engineering, Ar.C., Islamic Azad University, Arak, Iran.*

[*]**Corresponding author:** m-mirhoseini@iau-arak.ac.ir

Original Research

Abstract:

Soft clay soils with high water content and low bearing capacity pose serious challenges for geotechnical infrastructures, particularly in cold regions where repeated freeze-thaw cycles accelerate structural degradation. Although various nano-additives have been utilized to enhance soil stabilization, the synergistic effect of nano-titanium dioxide (nano-TiO_2) and carbon nanotubes (CNTs) in cement–silica fume systems has not yet been systematically evaluated. In this study, the combined influence of nano-TiO_2 and CNTs on the mechanical and durability properties of cement–silica fume stabilized soils was investigated through an extensive experimental program involving 243 specimens prepared with 12% cement and varying silica fume ($5-20\%$), nano-TiO_2 ($1-5\%$), and CNT ($0.15-0.45\%$) contents, cured for 7, 28, and 56 days. The specimens were subjected to 25 freeze–thaw cycles at a constant moisture content of 40%, exceeding the liquid limit of the soil.Results indicated that the silica fume–cement mixtures improved unconfined compressive strength (UCS) by an average of 85% compared to cement alone, while the incorporation of nano-TiO_2 and CNTs further increased UCS by up to 142%. Water absorption decreased by approximately 85%, and strength loss under freeze–thaw cycles was minimal. These findings highlight the novelty and practical significance of the nano-TiO_2–CNT composite in enhancing both the mechanical strength and frost durability of cement-stabilized soils, providing a sustainable approach to subgrade stabilization in cold climates.

Keywords:

Soft soils; Cement-stabilized soil; Silica fume, Nano-titanium dioxide; Carbon nanotubes; Freeze-thaw cycles; Unconfined compressive strength

Cite this article: Ajorloo, H., Mirhosseini, S.M., Hezavehi, E., Hassani Joshaghani, A. Synergistic Effect of Nano-TiO_2 and CNTs on the Mechanical and Microstructural Properties of Cement–Silica Fume Stabilized Soils under Freeze–Thaw Cycles. *Int. Nano Lett.* **14**(2), 142408 (2024).

1. Introduction

Soil stabilization using additives is a key topic in geotechnical engineering, aimed at improving the mechanical properties and durability of weak soils under various environmental conditions, particularly freeze-thaw cycles. This issue is of critical importance in both cold-region infrastructure projects and areas subject to significant temperature fluctuations. The impact of freeze-thaw cycles on the mechanical and hydraulic properties of soils, especially fine-grained soils, remains a major research challenge, demanding innovative solutions for sustainable construction practices.

The interaction between the stabilized soil matrix and reinforcement is paramount in applying these materials as reinforcement in geotechnical engineering. The interaction mechanism between the stabilized soil matrix and fibres can be highly complex and depends on the type of stabilized soil matrix and fibres. This section presents several laboratory methods for studying and evaluating the interaction between the stabilized soil matrix and fibers, using the specific laboratory standards relevant to this research on stabilized soil

matrix reinforcement. New applications of these methods are also discussed. The need for improvement in laboratory and experimental techniques to better investigate the interaction between the stabilized soil matrix and fibers is also highlighted.

Kahlor et al. investigated the effect of silica nanoparticles (SiO_2) on the geotechnical properties of fine-grained soils subjected to freeze-thaw cycles. Their study demonstrated that the addition of silica nanoparticles resulted in a decrease in maximum dry density and an increase in the optimum moisture content of the soil. Furthermore, unconfined compressive strength (UCS) improved significantly with optimal stabilization [1]. Wang et al. examined the mechanical properties of sandy clay soils (CGM) under varying effective stresses and freeze-thaw cycles. Their research indicated that the strength of sandy clay soils stabilizes after nine freeze-thaw cycles, after which the reduction in dynamic shear modulus has a weaker correlation with the number of cycles. Abbasi et al. explored the mechanical properties of weak sands during freeze-thaw cycles, utilizing unconfined compressive strength testing. Their findings, supported by scanning electron microscopy results, revealed that optimized samples retained $70-90\%$ of their initial unconfined compressive strength and stiffness after twelve freeze-thaw cycles [2, 3].

Zhou conducted a study examining the effects of freeze-thaw cycles on the mechanical and microscopic properties of coral sand under water infiltration conditions. Given that coral sand is employed as a construction material in the development of islands and marine structures, and due to its high calcium carbonate content (over 90%) and unique characteristics, it holds significant importance in geotechnical engineering. The findings of this study indicate that freezing and water infiltration substantially impact the mechanical and microscopic properties of coral sand. Ji Zhou et al. investigated the creep characteristics of cement-stabilized soils, demonstrating through microscopic analysis that freeze-thaw conditions considerably increase the deformation resulting from creep, while cement stabilization can mitigate this effect [4, 5].

Van's research focused on the influence of grain size on soil stability during freeze-thaw cycles, showing that finer soils exhibited reduced stability under these conditions. Specifically, the least reduction in stability was associated with grains sized between 2 and 4 millimeters, while the most significant decrease occurred in grains sized 0 to 1 millimeter. Furthermore, the effects of freeze-thaw cycles were found to be less pronounced in weaker-structured grains compared to those with better structural integrity [2, 3].

Yang et al. highlighted that freeze-thaw cycles generally lead to an increase in soil hydraulic conductivity. This increase is attributed to cracks formed due to drying and water absorption at the freeze interface, which subsequently serve as conduits for water flow when the ice melts. Konrad et al. observed that finer soils are more susceptible to the impacts of freezing and thawing, experiencing a significant increase in permeability, particularly notable during the initial freeze-thaw cycle, with effects that can persist through as many as 15 cycles. Ogata and colleagues investigated similar phenomena, concluding that freezing may enhance hydraulic permeability in conjunction with soil compaction, a finding that may initially appear paradoxical. In compacted dry soils, permeability was observed to increase by 2 to 3 times during freezing, while in compacted moist soils, the increase could be up to 100 times; these variations are attributed to changes in soil structure and degree of saturation [4–6].

Multiple studies have demonstrated that the impact of freeze-thaw cycles on the shear strength and mechanical behavior of soils is variable. Andersland et al. found that these cycles typically lead to a reduction in soil shear strength, attributing this effect to factors such as slow freezing rates, pre-consolidation pressure, the formation of new inter-particle bonds, and changes in the amount of free water present. In contrast, Andersland et al. reported that certain conditions could increase shear strength, including enhanced soil density and skeleton contraction. Additionally, Benoit emphasized that freezing pore water upon cooling below zero degrees Celsius results in particle separation and alterations in physical parameters such as porosity and water retention capacity, ultimately leading to reduced cohesion and mechanical strength. Furthermore, Lee et al. showed that the number of freeze-thaw cycles significantly affects the residue modulus of soils, with an increase in cycle count potentially causing a 25% to 60% reduction in the residue modulus across various soil samples. They also noted that compacted soils tend to expand, while loose soils become more compacted due to these cycles; however, this observation warrants further investigation [7–9].

Simonsen et al. conducted freeze-thaw experiments at temperatures ranging from -10 degrees Celsius to room temperature, demonstrating that the resilient modulus of soil decreased by 20% to 60%, depending on the type of soil, after the completion of the cycles. This initial reduction is most pronounced during the first cycle, and by the seventh cycle, the resilient modulus reaches its lowest value, decreasing by 18% to 27%, depending on the confining pressure. Graham et al. found that pre-consolidated soils exhibit a distinct peak in their modulus versus cycle number graphs, which diminishes due to loss of cohesion between particles as a result of freeze-thaw cycles and may even disappear. Additionally, Yarbaşı et al. investigated the effects of various additives, such as silica fume and ash, on the properties of granular soils under freeze-thaw cycles. Their findings revealed that the incorporation of these materials increases the optimal moisture content and reduces the maximum dry density of the soil, attributed to the increased specific surface area resulting from the presence of finer particles [10, 11].

Lajvardi and colleagues have conducted a series of studies investigating the impact of various additives on the mechanical behavior of cement-stabilized sands. One of these studies specifically focused on the simultaneous effects of fibers and natural zeolite on the failure characteristics of cemented sands. The results demonstrated that the incorporation of zeolite and fibers significantly improved post-peak behavior while reducing the brittleness of the specimens. Scanning Electron Microscopy (SEM) observations further confirmed

that zeolite enhances tensile strength and mitigates sudden failure of the samples by filling voids and coating the fibers. These findings suggest that the concurrent use of zeolite and fibers can lead to improved mechanical performance of cemented sands.Liu and colleagues investigated the effects of soil reinforcement on the dynamic properties of cement- and lime-modified clay in a cold climate region [12–17].

Soil improvement remains a fundamental pillar of geotechnical engineering, aimed at increasing bearing capacity, stiffness and durability while mitigating settlement, liquefaction risk and erosion-related failures. Conventional stabilization approaches-mechanical densification, lime/cement-based binders and geosynthetics-are effective in many contexts but often carry high material and carbon costs, and may require lengthy construction timeframes. In this context, nanotechnology has emerged as a complementary pathway: with relatively small dosages, engineered nanomaterials can modify pore-scale fabric and interparticle interactions and thereby influence macroscopic soil behaviour. Recent experimental and review studies report that nanoclays, nanosilica, metal-oxide nanoparticles and carbon-based nanoforms can improve stiffness, strength and durability across a variety of problematic soils [18, 19].

Mechanistically, the beneficial effects of nanoparticles on cementitious soil systems operate through several, often concurrent, routes: (i) micro-filling of sub-micron voids which reduces connected porosity; (ii) nucleation of hydration and pozzolanic products (e.g., accelerated C–S–H formation) that densify the binder matrix when used with cement or silica fume; (iii) electrochemical/colloidal interactions that promote particle flocculation or bridging; and (iv) modification of pore-water chemistry that can reduce compressibility and permeability. These pathways explain why low dosages of nanosilica or nanoclay frequently yield measurable increases in unconfined compressive strength and shear resistance, while certain metal-oxide nanoparticles (e.g., ZnO, TiO_2) have been associated with enhanced durability under cyclic wetting–drying or freeze–thaw regimes [18–20].

Beyond oxide nanoparticles, carbon-based nanomaterials (notably CNTs and graphene derivatives) introduce a different set of functionalities: when uniformly dispersed and effectively coupled with the binder matrix, these materials provide nano-scale reinforcement that can bridge microcracks, enhance tensile response and improve post-peak toughness. Similarly, photocatalytic oxides such as TiO_2 offer both microstructural benefits (nucleation, densification) and additional functionalities (e.g., photocatalysis) that may be relevant for contaminant attenuation in engineered fills. Nonetheless, practical adoption faces three recurring challenges: cost, reliable dispersion at scale, and uncertainty regarding long-term environmental fate and health impacts, especially for carbon nanomaterial [16, 18–21].

Despite substantial progress in soil stabilization research, significant knowledge gaps remain regarding the reinforcement mechanisms of weak soils treated with modern additives-particularly under harsh environmental conditions such as repeated freeze–thaw cycles. Previous studies have primarily focused on the individual effects of cement or silica fume on the unconfined compressive strength (UCS) of low-plasticity clays. However, the combined influence of cement–silica fume systems and nano-scale additives under cyclic freezing and thawing has received limited attention. The present study systematically investigates the role of cement and silica fume in improving the UCS and durability of soft clay soils, considering key parameters such as curing duration, cement content, and silica fume percentage. Subsequently, the study extends this framework to explore the synergistic incorporation of nano-titanium dioxide (nano-TiO_2) and carbon nanotubes (CNTs) into the cement–silica fume matrix to enhance both mechanical and microstructural performance under freeze–thaw conditions. The novelty of this research lies in: (i) conducting a comprehensive parametric analysis across multiple additive levels and curing periods; (ii) quantifying the synergistic effects of nano-TiO_2 and CNTs on UCS, water absorption, and microstructural densification; and (iii) establishing quantitative correlations between nano-additive content, strength improvement, and freeze–thaw resistance. These contributions provide new insights into the design of durable, eco-efficient, and sustainable soil stabilization systems, particularly for cold-region infrastructure where traditional binders often fail to maintain performance under cyclic thermal stresses.

Nano-TiO_2 improves hydration kinetics and refines microporosity through the formation of additional C-S-H gel, leading to enhanced strength and reduced permeability. Meanwhile, CNTs act as nano-reinforcement by bridging microcracks, increasing load transfer efficiency, and improving ductility. When incorporated together into cement–silica fume stabilized soils, these two nano-materials offer a complementary strengthening mechanism that yields superior frost resistance and durability compared with conventional additives.

2. Materials, methods, and experimental procedures

2.1 Materials and methods

This study utilized a low-plasticity clay soil (CL) classified according to the Unified Soil Classification System (USCS). The soil was obtained from a depth of 3 meters in the excavation area of an under-construction residential building in the Kianpars district of Ahvaz, Iran. The properties of the soil and silica fume used in this research are summarized in Table 1, and the particle size distribution of the soil is presented in figure 1.

Type II cement from the Dilijan Cement Factory in Iran was employed. This versatile cement, commonly used for general construction applications, is characterized for its moderate setting time and adequate strength development, making it a practical choice for a variety of construction projects.

Silica fume, is a pozzolanic material derived from producing ferrosilicon alloys. It is characterized by its excellent particle size and high reactivity with cement, leading to enhanced strength and durability properties in concrete. In this study, commercially available micro silica with a specific gravity of 2.2 and a Blaine fineness of 300,000 m^2/kg was

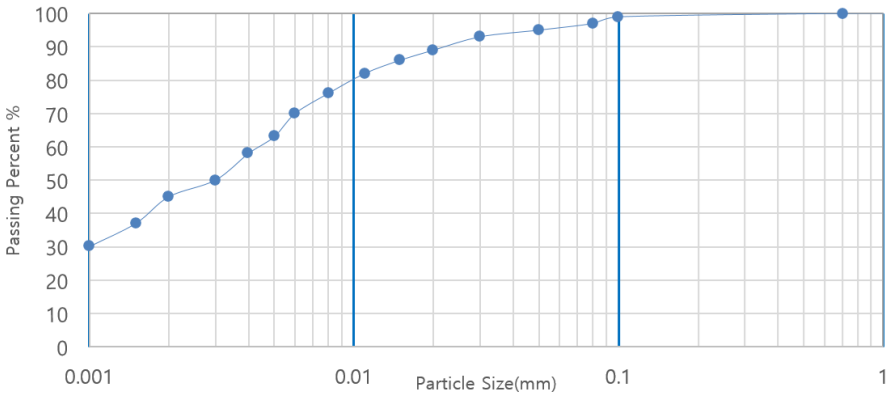

Figure 1. Particle size distribution curve of soil.

utilized. The properties soil, cement and silica fume used in this research are summarized in Table 1 to Table 3.

2.2 Preparation of specimens

2.2.1 Mix-design and sample numbering

The mix-design is summarized in Table 5. For clarity, silica fume contents used in this study are 0, 5, 10, 15 and 20% (by weight of cement). Carbon nanotube (CNT) contents are 0.00, 0.15, 0.25, 0.35 and 0.45% (by weight of cement). Nano-TiO_2 contents are 0, 1, 2, 3, 4 and 5% (by weight of cement). Each mix was prepared for three curing times (7, 28 and 56 days) with N = 3 replicates per curing time. Thus, total specimens = N_mix_codes × 3 × 3. The final total number of specimens prepared was 243.

2.2.2 CNT/nano-TiO_2 dispersion and mixing protocol

1. CNT pre-treatment and dispersion:

CNTs (functionalized, carboxylated) were weighed and dispersed in deionized water containing 0.1 wt.% sodium dodecyl sulfate (SDS) as surfactant. Dispersion was performed using a probe sonicator (e.g., 400 W, 20 kHz) at 40% amplitude for 30 min in an ice bath to avoid overheating.

2. nano-TiO_2 suspension:

nano-TiO_2 powder was added to the CNT suspension and sonicated for additional 10 min to ensure homogeneity.

3. Dry mixing:

Dry soil was sieved (2 mm) and mixed with silica fume in a mechanical mixer for 20 min to achieve uniform blending. Cement was then added and mixed for a further 10 min. The soil was air-dried and sieved through a 2 mm sieve to remove coarse particles. The optimum moisture content (OMC) and maximum dry density (MDD) of the soil were determined using the standard Proctor compaction test (ASTM D698).

4. Wet mixing & molding:

The CNT/TiO_2 suspension was added to the dry mix while stirring; mixing continued for 5 min at 60 rpm. The required mixing water was computed as: water_cement_requirement + water_for_target_moisture. The moist mix was placed into cylindrical molds (50 mm dia × 100 mm height), overfilled and compacted on a vibrating table for 30 s. Samples were demolded after 24 h and cured in a humidity chamber (20 ± 2 °C, RH ≈ 95%).
Cement-stabilized soil mixtures were prepared by mixing varying proportions of cement and silica fume with the soil. The cement content was fixed at 12%, while the silica fume

Table 1. Properties of soil.

Liquid limit	Plastic limit	Plastic index	Specific gravity of soil	Soil type
34%	18%	16%	2.62	CL

Table 2. Properties of cement.

(SiO_2)	(CaO)	(Fe_2O_3)	(AL_2O_3)	(SO_3)	(K_2O)
20.90%	65.02%	4.30%	5.0%	1.80%	0.60%

Table 3. Physical and chemical properties of silica fume.

Diameter (nm)	Specific surface area ($m^2$2/gr)	Purity	(SiO_2)%
11-13	200	98.17%	96.04%

content varied from 5% to 20% at increments of 5% by weight of cement. The mixtures were thoroughly blended until a uniform distribution of the additives was achieved. Dry soil was first passed through a No. 10 sieve [1] and weighed as required. Then, the amount of cement, CNT, nano-TiO_2 and silica fume needed was weighed according to the sample number in Table 3. Next, the silica fume was mixed with the dry soil and blended in a mixer for 20 minutes. Subsequently, the weighed cement was added to the mixed soil, and the mixer was operated for another 10 minutes to complete the mixing process [15]. During mixing, a lid was placed on the mixer container to prevent dust and loss of silica fume and cement during mixer rotation.

This study employed cement and silica fume simultaneously to stabilize soft clay soils. The soil moisture content was maintained at approximately 40% [1], and the cement content was fixed at 12% by weight of dry soil. For each cement content, silica fume was added at increments of 5% from 5% to 25%. Subsequently, carbon nanotubes (CNTs) were incorporated into the nano-titanium dioxide mixture at levels ranging from 0.15% to 0.45% of cement weight, and nano-titanium dioxide was added at 1% to 5% of cement weight. Three curing periods (TD) of 7, 28, and 56 days were considered for the specimens. The specimens were designated as A for the 7-day curing period, B for the 28-day curing period, and C for the 56-day curing period. These conditions were then repeated after the freeze-thaw cycles. Based on the parameters above, the specimens were prepared as shown in Table 2. The shape and mixing time of soil, cement, and silica fume were determined based on previous experience and the methods described in references [1, 7, 15].

As illustrated in figure 2, a set of four standard-sized molds was prepared. This ensemble consists of four cylindrical molds, each with a height of 100 mm and a diameter of 50 mm. Each cylindrical mold is composed of two half-cylinders connected by a clamp. During sample preparation, the clamp can be removed after 24 hours, and the sample can be extracted from the mold once it has hardened.

After mixing, the soil was removed from the mixer, and the required amount of water was added. The water needed for cement was first calculated, considering 31.25% of the soil weight to calculate the total water required. Then, the water needed to lubricate the soil was calculated based on the 40% moisture content. These two calculated water amounts were added to the mixed soil and manually mixed.

Before pouring the mixed soil, the mold walls were greased, and then the water-mixed soil was poured into three molds. The soil was poured higher than the mold height, and the set of molds was placed on a vibrating table for 30 seconds [1]. This step was crucial as it ensured the soil was evenly distributed in the molds and any entrapped air bubbles were removed, thereby achieving the desired soil density. The sample preparation steps are illustrated in figure 3.

The prepared soil mixtures were compacted to their respective MDD at the OMC in cylindrical molds with a diameter of 50 mm and a height of 100 mm. The compacted specimens were then cured in a moist room at 20 °C and relative humidity of 95% for 7, 28, and 56 days. Once prepared, the specimens were placed in a room at a temperature of $20-22$ °C for 24 hours to gain initial strength. The specimens were then removed from the molds, wrapped in plastic, and labelled with their respective numbers. The specimens were stored in the same room until the complete curing period.

2.3 Experimental procedures

After the curing process, the specimens were subjected to a series of freeze-thaw cycles. This was a deliberate step in our experiment, aimed at simulating the potential effects of cold weather conditions on the specimens. The freeze-thaw cycles were conducted in a temperature-controlled chamber, with the specimens being exposed to temperatures of -18 °C for 12 hours and 20 °C for 12 hours, followed by a rest period of 6 hours. Each specimen endured a total of 25 such cycles.

The UCS of the specimens before and after freeze-thaw cycles was determined using a standard unconfined compressive strength test (ASTM D2166). The specimens were loaded at a constant strain rate until failure, and the maximum load was recorded. The load was measured in Newtons (dN = kgf), and the measurement accuracy was 0.001 kg. According to ASTM D2166, the loading rate should be between 0.5% and 2% of the longitudinal strain. Therefore, the loading rate in this test was set to 0.5 mm/min. The UCS was calculated by dividing the maximum load by the cross-sectional area of the specimen.

The water absorption of the specimens before and after freeze-thaw cycles was determined by submerging them in water for 24 hours and measuring their weight gain. The water absorption was calculated as the percentage increase

Figure 2. Standard-sized molds.

Figure 3. Sample preparation.

in weight compared to the specimen's dry weight. The mix design is shown in Table 5.

The experimental data were meticulously analyzed to investigate the effects of silica fume content, freeze-thaw cycles, and curing period on the UCS and water absorption of the cement-stabilized soil mixtures. The required standards for testing the specimens are summarized in Table 4.

The unconfined compression test (UCS) was performed to quantify mechanical improvements in strength and durability. Scanning electron microscopy (SEM) was employed to assess microstructural evolution, including pore refinement and interparticle bonding. Additionally, X-ray diffraction (XRD) analysis was conducted to evaluate mineralogical transformations and the formation of pozzolanic reaction products induced by nano-TiO_2 and CNT additives. Together, these tests provide an integrated characterization framework linking mechanical behavior to microstructural mechanisms.

2.4 Equipment, measurements and data analysis

Unconfined compressive strength (UCS) tests were performed using an STM-400 universal testing machine equipped with a 400 kN load cell. Specimens were loaded at a constant displacement rate of 0.5 mm/min until failure; axial strain was recorded using an external LVDT. Freeze–thaw cycles were applied in a programmable climatic chamber (Model: Freezing and Thawing ApparatusCo725), using the following profile: −18 °C for 12 h →

Table 4. Standard test methods.

Standard	Test
ASTM D422	Standard Test Method for Particle-Size Analysis
ASTM D4318	Standard Test Methods for Liquid Limit, Plastic Limit and Plasticity Index of Soils
ASTM D2216	Standard Test Methods for Lab Determination of Water Content of Soil
ASTM D2487	Standard Practice for Classification of Soils for Engineering Purposes (Unified Soil Classification System)
ASTM D854	Standard Test Methods for Specific Gravity of Soil Solids by the Water Displacement Method
ASTM D2166	Standard Test Method for Unconfined Compressive Strength of Cohesive Soil
ASTM F3419-22	Standard Test Method for Mineral Characterization of Equine Surface Materials by X-Ray Diffraction (XRD) Techniques
ASTM D 560	Standard Test Methods for Freezing and Thawing Compacted Soil-Cement Mixtures
ASTM F1372-93	Standard Test Method for Scanning Electron Microscope (SEM)
ASTM D698	Standard Test Methods for Laboratory Compaction of Soil Standard

ramp to +20 °C in 1 h → +20 °C for 12 h → rest 6 h (one cycle). A total of 25 cycles were applied to the specimens selected for durability testing. SEM imaging was carried out on a [SEM Phenom ProX] at $10-15$ kV after gold sputtering; XRD patterns were recorded on a PANalytical X'Pert PRO (Cu-Kα, $\lambda = 1.5406$ Å) in the 2θ range $5°$ $- 70°$ with $0.02°$ step size. Water absorption (VWA) was measured by submerging specimens in deionized water for 24 h and calculating the percent mass gain: VWA (%) = (m_wet − m_dry)/m_dry × 100.

3. Result

3.1 Unconfined compressive strength

As illustrated in figure 4, the condition of the specimens after failure is shown. The failure occurred along the height of the specimen, indicating a particular mode of failure linked to the hardening and strengthening of the stabilized soil. Continuous monitoring during the experiment revealed that this type of failure is characteristic of well-stabilized materials, showcasing the effectiveness of the treatment applied. In contrast, if the specimen were soft, failure would not occur; instead, under continuous loading, we would observe an increase in strain and a barrel-shaped appearance of the specimen. This behavior highlights the importance of adequate stabilization in preventing catastrophic failures in soft soils. The increase in strength in stabilized soil is primarily attributed to the cement and silica fume's role in creating bonds between clay particles [7]. This enhanced bonding not only improves the mechanical properties of the soil but also contributes to reduced permeability, making the stabilized soil more resilient against environmental factors.

The UCS results for the Samples, categorized by similar curing periods, are presented in figure 5. This table includes not only the UCS values measured after freeze-thaw cycles but also the corresponding volumetric water absorption percentages, providing a comprehensive view of the specimens' performance under varying conditions. These results are crucial for assessing the durability and stability of the stabilized soil, as higher UCS values generally indicate improved mechanical strength, while lower water absorption percentages suggest better resistance to moisture-related degradation.

The freeze-thaw cycles caused a slight reduction in the UCS of the specimens, with the magnitude of the reduction decreasing with increasing curing period and silica fume content. Specifically, the UCS values decreased by approximately 4% after 9 freeze-thaw cycles, indicating a correlation between the duration of curing and the degree of preservation of strength. This decrease in strength is likely due to microcracks induced by the thermal expansion and contraction of water and air within the soil matrix. However, the overall strength retention of the specimens after freeze-thaw cycles remained relatively high, indicating the effectiveness of the cement-silica fume-CNT-nano-TiO_2 stabilization system in enhancing the freeze-thaw resistance of the soil.

All specimens were compacted at a 40% water content, which exceeds the liquid limit of the soil and provides sufficient pore water to participate in freeze–thaw action. After curing, the moisture content reduced to approximately 20%, resulting in partially saturated conditions representative of subgrades in cold climates. During freezing, the remaining

Figure 4. Unconfined compressive strength sample.

Table 5. Mix design.

Mix Design Code	Cement %	Silica Fume %	Nano-titanium dioxide (nano-TiO_2)%	Carbon Nanotube (CNT)%
CM1	0	0	0	0
CM2	12	0	0	0
CM3	12	5	0	0
CM4	12	10	0	0
CM5	12	15	0	0
CM6	12	20	0	0
CM7	12	15	1	0
CM8	12	15	1	0
CM9	12	15	3	0
CM10	12	15	4	0
CM11	12	15	5	0
CM12	12	15	0	0.15
CM13	12	15	0	0.25
CM14	12	15	0	0.35
CM15	12	15	0	0.45
CM16	12	15	1	0.35
CM17	12	15	2	0.35
CM18	12	15	3	0.35
CM19	12	15	4	0.35
CM20	12	15	5	0.35

pore water expands, inducing frost-related stresses and affecting strength retention.

Figure 6 clearly illustrates that specimens CM18 and CM20 exhibit the lowest Volumetric Water Absorption (VWA), while the control specimens (CM0) and CM2 display the highest VWA. The volumetric water absorption (VWA) decreased from approximately 5.1% in the control mix to about 1.0% in the optimized nano-modified mix, corresponding to an $80-85\%$ reduction. The reduced VWA in specimens CM18 and CM20 prepared using the CNT-nano-TiO_2 composite can be attributed to the formation of solid cross-links and a robust metal complex. The carboxylated nano-TiO_2 in these specimens forms a COOH group upon interaction with CNTs, forming strong cross-links. Additionally, nano-TiO_2 interacts with OH groups to create a robust metal complex. This complex enhances the crystalline properties and reduces moisture absorption. Incorporating nano-TiO_2 further reduces VWA, as observed in specimen CM20, where the VWA drops to 1%.

This reduction in VWA is particularly evident compared to specimens containing only CNTs. In the latter case, nano-TiO_2 acts solely as a matrix within the soil, unable to form a metal complex due to the absence of strong bonds. Consequently, it cannot induce crystallinity and reduce water

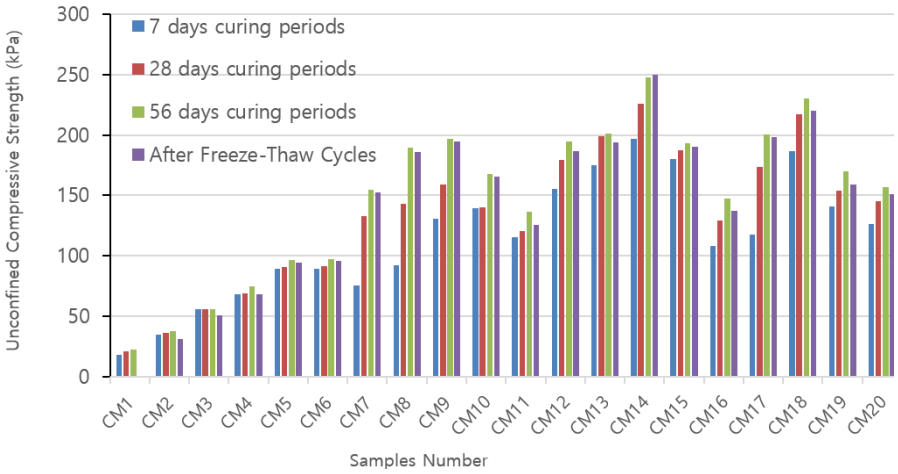

Figure 5. UCS results for the samples.

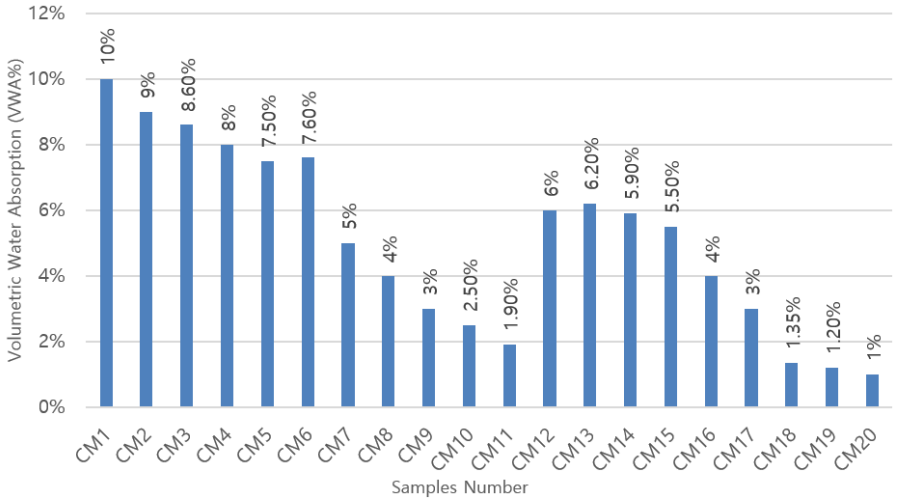

Figure 6. Volumetric water absorption (VWA) for the samples.

absorption from the CNT-nano-TiO_2 composite.

3.2 Interpretation of X-ray diffraction (XRD) patterns of nano-titanium dioxide and carbon nanotubes

Three samples were subjected to X-ray diffraction (XRD) analysis to investigate the effect of adding nano-titanium dioxide (nano-TiO_2) and carbon nanotubes (CNTs) on the microstructure of the stabilized soil. The XRD patterns shown in figure 7 illustrate the crystalline structures of the three analyzed samples: Sample a (with nano-TiO_2), Sample b (with CNTs), and Sample c (composite of nano-TiO_2 and CNTs). Each coloured line corresponds to a different sample, with distinctive peak characteristics indicating the phase composition of the materials. The XRD patterns of the three samples exhibit the characteristic peaks of quartz, calcite, and clay minerals, indicating their presence in the stabilized soil. The intensity of the quartz and calcite peaks is slightly higher in Sample a than in Samples b and c. This observation suggests that nano-TiO_2 facilitated the crystallization of quartz and calcite during the curing process. The XRD patterns, depicted in figure 7, provide valuable insights into the materials' phase composition and microstructural characteristics.

Sample a: Nano-TiO_2

The XRD pattern for Sample 1 (displayed in red) reveals distinct peaks, characteristic of the anatase phase of titanium dioxide around 2θ values of 25.3°, 37.9°, and 48.0°. These sharp peaks indicate a well-crystallized structure, suggesting high purity and effective integration of nano-TiO_2 within the matrix, improving its mechanical and chemical stability. This phase is known for its photocatalytic activity and potential to improve soil stabilization.

Sample b: Carbon Nanotubes (CNTs)

The XRD pattern for Sample 2 (shown in blue) exhibits a broad and weak peak around 2θ values of 25-30° corresponding to the (002) reflection of CNTs.The intensity of this peak is comparatively weak, suggesting a low dispersion of CNTs within the soil matrix. This diffuse peak is typical for amorphous carbon materials. It indicates the presence of structural defects, suggesting that these CNTs are likely not fully crystallized, which is consistent with existing literature on carbon nanotube synthesis. This broadening indicates the presence of structural defects or various carbon species in the sample, which may affect the mechanical properties of the stabilized soil.

Sample c: Composite of Nano-TiO_2 and CNTs

The XRD pattern for Sample 3 (illustrated in green) combines features from both previous samples. Also, the quartz and calcite peaks are slightly more intense than in Sample 2. While the characteristic peaks of the anatase phase remain, there may also be indications of a potential interaction or synergy between the nano-TiO_2 and the CNTs. This could suggest improved dispersion of nanoparticles in the soil matrix, leading to enhanced performance metrics due to the composite material's combined mechanical and chemical properties.

The XRD analysis provides critical insights into the crystalline structures of the incorporated nanomaterials. The unique characteristics of each diffraction pattern reinforce the hypothesis that adding nano-TiO_2 and CNTs can significantly improve the microstructural properties of stabilized soil. Nano-TiO_2 may have facilitated the crystallization of quartz and calcite, while CNTs may have contributed to the reinforcement of the soil matrix. These findings highlight the significance of understanding the interaction between different nanomaterials and their roles in enhancing the performance of geotechnical applications.

The effect of the curing period is evident in the increased slope and ultimate stress of the stress-strain curves for specimens with more extended curing periods. This observation indicates that the pozzolanic reaction and C-S-H gel formation progress over time, leading to a denser and more cohesive soil matrix.

The graphs in figure 6 show the increase in the specimens' UCS over different curing periods. The strength gain rate for the 7-day curing period was approximately 256%, 176% for the 14-day curing period, and 96% for the 28-day curing period.

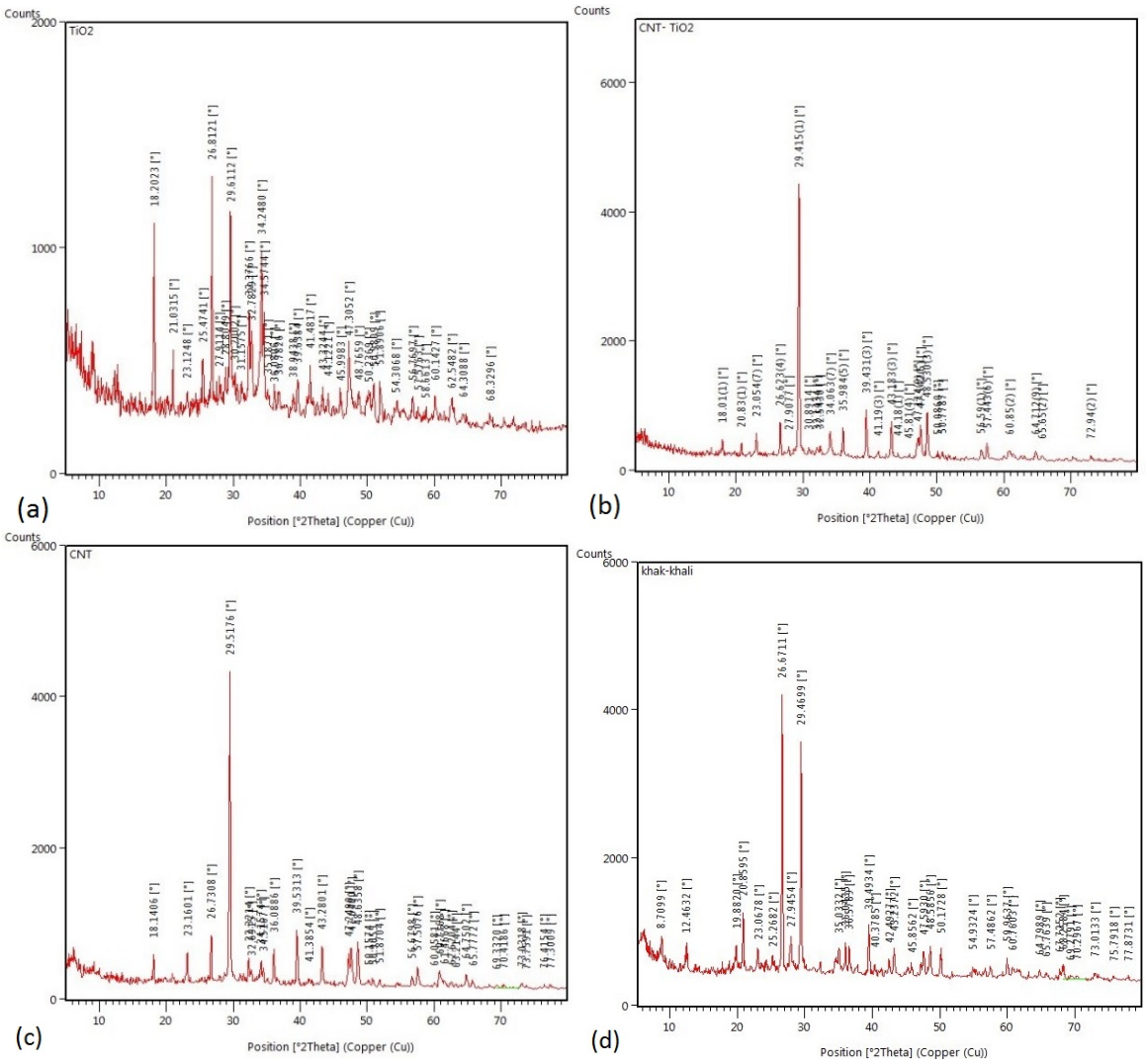

Figure 7. XRD pattern of the samples. (a) TiO_2, (b) CNT + TiO_2, (c) CNT, (d) no additive.

As observed, the strength gain rate decreases with increasing curing period. This can be attributed to the ratio of cement to silica fume used. Since the weight of cement is more than ten times that of silica fume, the curing time of cement is dominant. This is because most cement hydration occurs in the first 7 days. Additionally, silica fume accelerates cement hydration due to its high surface energy. Naturally, the strength growth rate decreases as the curing time continues and the hydration process is completed.

The effect of silica fume content is also evident in the steeper slopes and higher ultimate stresses of the stress-strain curves for specimens with higher silica fume contents. This observation suggests that the pozzolanic reaction is more pronounced with increasing silica fume content, leading to a more significant enhancement in strength and ductility. The increase in specimen strength with increasing silica fume content is due to the pozzolanic reaction between silica fume and free lime released during the hydration process, producing more calcium silicate hydrate (C-S-H). This, in turn, improves the mechanical properties of the soil. In most specimens, the strength decreases after increasing silica fume beyond 2.1%. This decrease in strength could be due to the agglomeration of nano-silica particles. As the number of nano-particles with high specific surface area increases, more particles are accommodated in a fixed volume.

Figure 6 demonstrates that the UCS values of the specimens significantly increased with increasing curing period and silica fume content. This observation indicates that the bonds between particles become complete as time progresses, enhancing strength. This enhancement in strength is attributed to the pozzolanic reaction between cement and silica fume, leading to calcium silicate hydrates (C-S-H) gels that densify the soil matrix and enhance interparticle bonding. Adding carbon nanotubes (CNTs) and nano-titanium dioxide (nano-TiO_2) further improved strength by providing additional nucleation sites for C-S-H gel formation and reinforcing the soil matrix.

Further insights can be gained from the graphs in figure 6. The highest UCS values were observed in specimens CM18 and CM14, while the control specimens (CM0) and CM2 exhibited the lowest UCS. In specimen CM14, only 0.35% carbon nanotubes were used without nano-titania, whereas in specimen CM18, in addition to 0.35% carbon nanotubes, 3% nano-titania was also used, and this composite exhibited remarkable UCS. The reason for this lies in the polygonal

dispersion of carbon nanotubes on the soil surface. These tubes not only have helical symmetry but also possess translational symmetry along the axis of the tube. When carbon nanotubes and nano-titania are combined and carboxylic and COOH groups are formed, this remarkable strength is also observed in specimen CM18. This represents an increase of approximately 146% compared to the control specimen.

3.3 Scanning electron microscope (SEM)

The ASTM F1372-93 standard was utilized to conduct microscopic imaging of the samples. According to figure 8 a, the soil is free of nanomaterials. Figure 8 b is composed solely of titanium dioxide nanoparticles, while figure 8 c is entirely combined with carbon nanotubes. In contrast, figure 8 d exhibits a composite of carbon nanotubes and titanium dioxide nanoparticles.

Performance of titanium dioxide nanoparticles

Figure 8 b, which consists solely of titanium dioxide nanoparticles, shows a uniform distribution of nanoparticles, positively affecting the physical properties of the samples. However, the presence of metallic linkages (metal complexes) in these samples contributes to the formation of strong cross-links. It is important to note that while this increase in metallic linkages is due to the rising concentration of titanium dioxide nanoparticles, it may lead to excessive brittleness of the samples, ultimately reducing the unconfined compressive strength.

Performance of carbon nanotubes

In figure 8 c, the distribution of carbon nanotubes is more uniform across the surface of the samples. This uniform distribution facilitates the formation of strong bonds between the cement particles and the carbon nanotubes, consequently leading to an increase in unconfined compressive strength. This effect reflects the positive impact of carbon nanotubes on the mechanical properties of these samples, indicating a reinforced interaction between the nanotubes and the cement particles.

Performance of the composite of titanium dioxide nanoparticles and carbon nanotubes

Figure 8 d illustrates that due to the presence of carboxylic groups, the distribution of carbon nanotubes is not uniform. This aids in the formation of carboxylic bonds between the nanotubes and the soil matrix. These linkages signify the existence of strong cross-links that improve the composite's mechanical properties. Therefore, this non-uniform distribution of carbon nanotubes contributes to enhancing the mechanical connections among the components.
Although CNTs exhibit partial agglomeration, their carboxyl functional groups enable chemical bonding with TiO_2 particles, enhancing interfacial strength.

Overall observations

The SEM images provide valuable insights into the microstructure of the stabilized soil and its relationship with mechanical properties. The uniform distribution of CNTs in CNT-only specimens and the formation of strong cross-

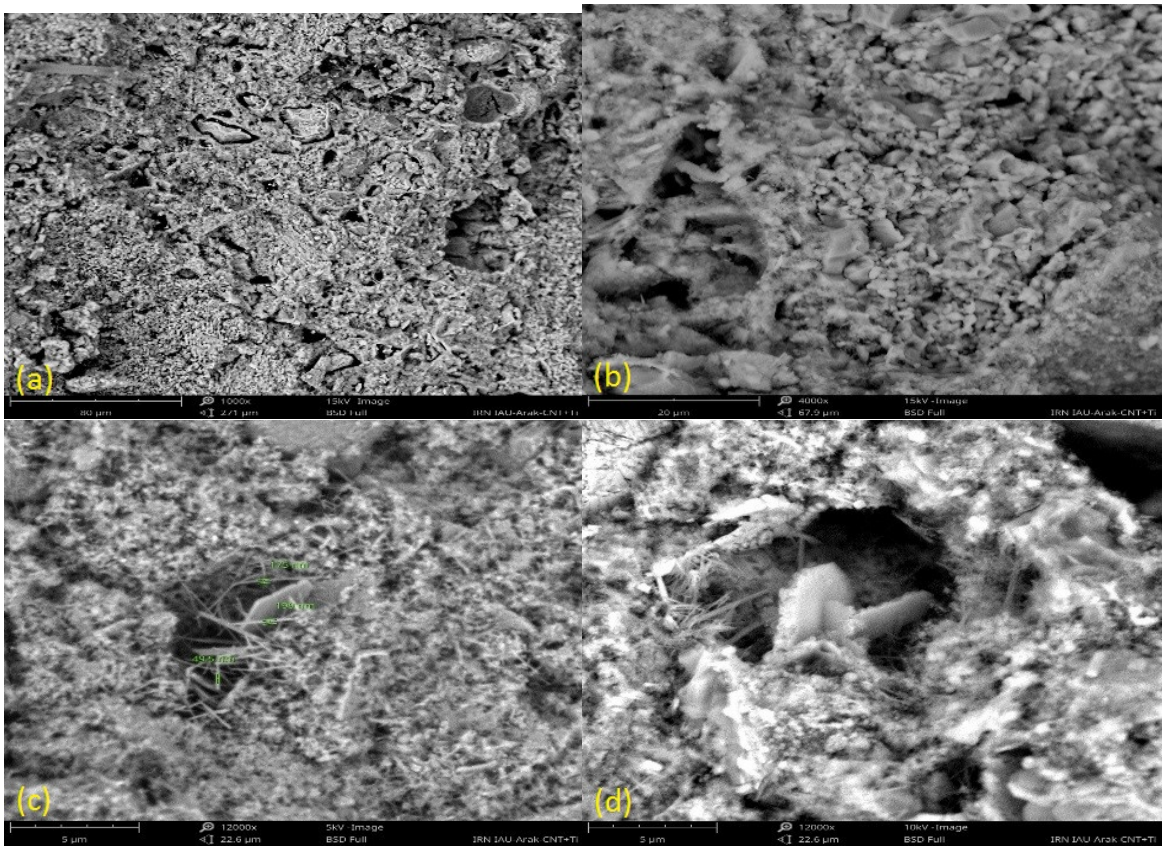

Figure 8. SEM micrographs of stabilized soils with different nano-additives. (a) no additive, (b) TiO_2, (c) CNT, (d) CNT + TiO_2.

links in CNT-nano-TiO_2 composite specimens contribute to the enhanced UCS observed in these specimens. The SEM and XRD results confirmed the microstructural mechanisms responsible for improved mechanical behavior. Specifically, SEM observations demonstrated refined pore structure, improved interparticle bonding, and CNT-induced crack-bridging, while XRD patterns showed enhanced C–S–H formation driven by nano-TiO_2-assisted pozzolanic reactions. These microstructural enhancements directly support the significant UCS retention observed after freeze–thaw cycles.

3.4 Mechanisms behind the observed strength gain and freeze–thaw resistance

The experimental results indicate two complementary mechanisms driving the enhanced performance of the cement–microsilica–nano-TiO_2–CNT system: (1) microstructural densification via accelerated hydration and pozzolanic reactions, and (2) nanomechanical reinforcement by CNTs.

First, microsilica and nano-TiO_2 act as high-surface-area nucleation sites that promote the formation of C–S–H and other hydration products. This is supported by the XRD patterns (Fig. 7), which show increased intensity of hydration-related peaks in TiO_2-containing specimens. Quantitatively, an XRD-based index of crystallinity, for example, integrated intensity of C–S–H-related peaks normalized to quartz, can be calculated and correlated with UCS to demonstrate this effect more clearly. The expected consequence is a reduction in connected porosity and capillary pathways, consistent with the substantial reductions in volumetric water absorption reported for CM18/CM20 (VWA lowered to $\approx 1\%$ in CM20).

Second, CNTs function as nano-reinforcements: when well-dispersed they bridge microcracks, enhance tensile resistance at the microscale, and redistribute stresses, which increases both peak strength and post-peak energy absorption. SEM micrographs (Fig. 8) document CNT presence at interparticle contacts; image analysis (e.g., quantifying crack length density and CNT pull-out features) will provide metrics to link this micro-reinforcement to UCS gains. The observed up to $\approx 142\%$ increase in UCS for nano-enhanced mixes (relative to cement-only control) is therefore attributable to both matrix densification and nano-reinforcement working in synergy.

Lastly, the improved freeze–thaw resistance can be mechanistically explained: reduced free water (lower VWA) and lower connectivity of capillary pores limit ice lens formation and pore pressure build-up during freezing, while the CNT network resists microcrack propagation during thawing. The modest UCS reductions after cyclic loading (e.g., $\approx 4\%$ after intermediate cycles as reported) are consistent with this combined protective mechanism, though full durability assessment under field-relevant saturation regimes will require additional testing. Importantly, assertions about chemical bonding between TiO_2 and CNTs (e.g., COOH formation) require spectroscopic confirmation (FTIR/XPS); until such data are provided, we rephrase these interactions as plausible chemical/physical synergies supported by microstructural evidence.

3.5 Comparison with previous studies

A number of previous investigations have addressed the use of pozzolans and nano-scale additives for improving soil mechanical properties under freeze–thaw loading [1, 12, 16]. Kalhor et al. [1] demonstrated that nano-SiO_2 increased UCS and modified compaction characteristics for fine soils under freeze–thaw; however, their study focused on a single nano-additive and did not examine CNTs or combined nano-oxide/CNT systems. Liu et al. [16] reported improvements in small-strain stiffness for cement–lime modified clays, yet indicated sensitivity to freeze–thaw exposure when aggregate saturation is high.

Compared with these studies, our results show substantially larger UCS enhancements and markedly lower volumetric water absorption. We attribute the improved performance to three mechanistic factors, supported by our SEM/XRD observations: (1) nucleation and accelerated C-S-H formation promoted by nano-TiO_2 and high microsilica content (denser matrix and reduced capillary porosity); (2) nanotube-mediated crack-bridging and stress redistribution, which enhance post-peak toughness and resistance to microcrack propagation during freeze–thaw; and (3) improved dispersion of the nano-additives (sonication + surfactant), which reduces agglomeration and maximizes effective surface area. This comparative analysis confirms that the combined nano-TiO_2 + CNT strategy offers advantages beyond single-additive approaches reported previously.

4. Conclusion

This study systematically investigated the synergistic influence of nano-titanium dioxide (nano-TiO_2) and carbon nanotubes (CNTs) on the mechanical and durability performance of cement–silica fume stabilized soft clay under freeze–thaw cycles. A total of 243 specimens with 12% cement, varying silica fume ($5-20\%$), nano-TiO_2 ($1-5\%$), and CNT ($0.15-0.45\%$) contents were tested after 7, 28, and 56 days of curing.

The results demonstrated that incorporating silica fume with cement increased the unconfined compressive strength (UCS) by an average of 85% after 28 days, while also reducing cement demand by approximately 4%. The addition of nano-TiO_2 and CNTs further enhanced the UCS by up to 142% compared with the cement-only mix. The volumetric water absorption (VWA) was significantly reduced—by about $80-85\%$ and the specimens retained most of their strength after 25 freeze–thaw cycles, confirming the composite's superior frost resistance and moisture stability.

The observed improvements arise from two complementary mechanisms: (i) nano-TiO_2 and silica fume accelerate hydration and pozzolanic reactions, refining pore structures and producing a denser C–S–H matrix, while (ii) CNTs bridge microcracks and enhance stress transfer, leading to higher strength and improved durability. These microstructural synergies were supported by SEM and XRD observations showing increased matrix compactness and higher crystallinity in nano-modified specimens.

From an engineering standpoint, the proposed nano-TiO_2–CNT–microsilica–cement system offers an effective and sustainable approach for stabilizing soft soils in cold climates. The approach not only improves mechanical integrity and freeze–thaw durability, but also supports cement reduction and potentially lowers the carbon footprint of soil stabilization projects.

Future work should incorporate spectroscopic (FTIR/XPS) and quantitative image analyses to verify the hypothesized nano-scale interactions, and conduct long-term field studies under varying saturation conditions to translate the laboratory findings into practical design recommendations for infrastructure foundations and subgrades in cold regions.

Authors Contribution
All authors have contributed equally to prepare the paper.

Availability of data and materials
The datasets generated during and/or analyzed during the current study are available from the corresponding author on reasonable request.

Conflict of interests
The authors declare that they have no known competing financial interests or personal relationships that could have appeared to influence the work reported in this paper.

References

[1] A. Kalhor, M. Ghazavi, M. Roustaei, and S. M. Mirhosseini. Influence of nano-SiO_2 on geotechnical properties of fine soils subjected to freeze-thaw cycles. *Cold Reg Sci Technol*, **161**:129–36, (2019). DOI: https://doi.org/10.1016/j.coldregions.2019.03.011.

[2] VAN KLAVEREN RW. Hydraulic erosion resistance of thawing soils. Washington State University. (1987).

[3] J. Qi, W. Ma, and C. Song. Influence of freeze–thaw on engineering properties of a silty soil. *Cold Reg Sci Technol*, **53**:397–404, (2008). DOI: https://doi.org/10.1016/j.coldregions.2007.05.010.

[4] C. S. Yang, P. He, G. D. Cheng, Y. L. Zhu, and S. P. Zhao. Testing study on influence of freezing and thawing on dry density and water content of soil. *Chinese Journal of Rock Mechanics and Engineering*, **22**:2695–9, (2003).

[5] J.-M. Konrad and N. R. Morgenstern. A mechanistic theory of ice lens formation in fine-grained soils. . *Canadian Geotechnical Journal*, **24**:473–86, (2023). DOI: https://doi.org/1980;17:. https://doi.org/10.1139/t80-056.

[6] N. Ogata. Effect of freezing-thawing on the mechanical properties of soil. . *Proceedings of the 4th International Symposium on Ground Freezing*, :201–7, (1985).

[7] G. R. Benoit and W. B. Voorhees. Effect of freeze–thaw activity on water retention, hydraulic conductivity, density, and surface strength of two soils frozen at high water content. (1990).

[8] W. Lee, N. C. Bohra, A. G. Altschaeffl, and T. D. White. Resilient Modulus of Cohesive Soils. *Journal of Geotechnical and Geoenvironmental Engineering*, **123**:1311–6, (1997). DOI: https://doi.org/10.1061/(ASCE)1090-0241.

[9] O. B. Andersland and D. M. Anderson. Geotechnical engineering for cold regions. *McGraw Hill*, , (1978). DOI: https://doi.org/10.hdl.handle.net/2346/98317.

[10] E. Simonsen and U. Isacsson. Soil behavior during freezing and thawing using variable and constant confining pressure triaxial tests. *Canadian Geotechnical Journal*, **38**:863–75.

[11] J. Graham. Au VCS. Effects of freeze–thaw and softening on a natural clay at low stresses. *Canadian Geotechnical Journal*, **22**: 69–78, (1985). DOI: https://doi.org/10.1139/t85-007.

[12] S. H. Jafari and S. H. Lajevardi. Influence of freeze–thaw cycles on strength and small strain shear modulus of fine-grained soils stabilized with nano-SiO_2 and lime using bender element tests. . *Bulletin of Engineering Geology and the Environment*, **81**:234, (2022). DOI: https://doi.org/10.1007/s10064-022-02730-y.

[13] Y. Heidarizadeh, S. H. Lajevardi, M. Sharifipour, and Kamalian M. Experimental characterization of the small strain shear modulus of soft clay stabilized with cement and nano-SiO_2 using bender element tests. *Bulletin of Engineering Geology and the Environment*, **80**: 2523–34, (2021). DOI: https://doi.org/10.1007/s10064-020-02096-z.

[14] P. Rabbani, A. Tolooiyan, S. H. Lajevardi, Y. Daghigh, and M. Falah. The Effect of the Depth of Cutter Soil Mixing on the Compressive Behavior of Soft Clay Treated by Alkali-Activated Slag. *KSCE Journal of Civil Engineering*, **23**:4237–49, (2019). DOI: https://doi.org/10.1007/s12205-019-0335-4.

[15] A. Esfandyaripour, S. H. Lajevardi, and H. MolaAbasi. An experimental study to examine the effect of fiber and natural pozzolan on the failure characteristics of a cement-treated sand. *Proceedings of the Institution of Civil Engineers-Ground Improvement*, :1–29, (2023). DOI: https://doi.org/10.1680/jgrim.22.00024.

[16] J. Liu, T. Wang, and Y. Tian. Experimental study of the dynamic properties of cement-and lime-modified clay soils subjected to freeze–thaw cycles. *Cold Reg Sci Technol*, **61**:29–33, (2010). DOI: https://doi.org/10.1016/j.coldregions.2010.01.002.

[17] P. Rabbani, S. H. Lajevardi, A. Tolooiyan, Y. Daghigh, and M. Falah. Effect of Cutter Soil Mixing (CSM) method and curing pressures on the tensile strength of a treated soft clay. *Heliyon*, **5**, (2019). DOI: https://doi.org/10.1016/j.heliyon.2019.e02186.

[18] G. Aksu and T. Eskisar. The geomechanical properties of soils treated with nanosilica particles. *Journal of Rock Mechanics and Geotechnical Engineering*, **15**:954–69, (2023). DOI: https://doi.org/10.1016/j.jrmge.2022.06.013.

[19] H. R. Akbari, H. Sharafi, and A. R. Goodarzi. Effect of polypropylene fiber inclusion in kaolin clay stabilized with lime and nano-zeolite considering temperatures of 20 and 40 °C. *Bulletin of Engineering Geology and the Environment*, **80**:1841–55.

[20] H. Ahmadi. Experimental study of the effect of nano-additives on the stiffness of cemented fine sand. *International Journal of Geotechnical Engineering*, **15**:433–46, (2021). DOI: https://doi.org/10.1080/19386362.2019.1663067.

[21] K. Tavakol, M. Bayat, B. Nadi, and R. Ajalloeian. Combined Influences of Cement, Rice Husk Ash and Fibre on the Mechanical Characteristics of a Calcareous Sand. . *KSCE Journal of Civil Engineering*, **27**:3729–39, (2023). DOI: https://doi.org/10.1007/s12205-023-0695-7.